Journal of
Materials Chemistry A

ROYAL SOCIETY
OF CHEMISTRY

REVIEW

View Article Online
View Journal | View Issue

Cite this: *J. Mater. Chem. A*, 2020, **8**, 1545

Aqueous electrocatalytic N_2 reduction for ambient NH_3 synthesis: recent advances in catalyst development and performance improvement

Xiaojuan Zhu, Jr,[ab] Shiyong Mou,[a] Qiling Peng,[a] Qian Liu,[a] Yonglan Luo,[b] Guang Chen,[c] Shuyan Gao[d] and Xuping Sun*[a]

Received 28th November 2019
Accepted 11th December 2019

DOI: 10.1039/c9ta13044f

rsc.li/materials-a

Electrochemical N_2 reduction has emerged as an environmentally benign alternative to the Haber–Bosch process for sustainable NH_3 synthesis under ambient reaction conditions, and considerable recent attention has focused on electrocatalytic NH_3 synthesis from N_2 and H_2O in aqueous media. In this Minireview, we summarize the recent advances in the development of electrocatalysts for the N_2 reduction reaction (NRR). Strategies to boost the NRR performances are also discussed. Perspectives for further research directions are provided finally.

Xuping Sun received his PhD degree from the Changchun Institute of Applied Chemistry (CIAC), Chinese Academy of Sciences in 2006. During 2006–2009, he carried out postdoctoral research at Konstanz University, the University of Toronto, and Purdue University. In 2010, he started his independent research career as a full professor at the CIAC and then moved to Sichuan University in 2015. In 2018, he joined the University of Electronic Science and Technology of China where he founded the Research Center of Nanocatalysis & Sensing. He was recognized as a highly cited researcher (2018 & 2019) in areas of both chemistry and materials science by Clarivate Analytics. He has published over 440 papers with total citations over 32 000 and an h-index of 93. His research mainly focuses on rational design of functional nanostructures for electrocatalysis and sensing applications.

1. Introduction

NH_3 is not only widely utilized as an essential activated nitrogen source to manufacture agricultural fertilizers, dyes, polymers, explosives, *etc.*, but also provides a carbon-free chemical energy carrier solution for the transportation sector.[1–3] As the dominant route for industrial-scale NH_3 production using N_2 and H_2 as the feed gases, the century-old Haber–Bosch process suffers from harsh reaction conditions, complicated factory infrastructure, high energy consumption, and serious CO_2 emissions.[4] One alternative approach to solve the NH_3 synthesis problem is to use electricity to drive the NH_3 production reaction,[5] and this electrically driven process is compatible with intermittent operation and enables utilization of renewable electricity without needing transmission capacity expansion. Electrochemical N_2 reduction has emerged as an attractive method for artificial N_2-to-NH_3 conversion under ambient conditions; however it is severely challenged by N_2 activation and needs efficient electrocatalysts to break the rather inert molecular structure of N_2 with an extremely high bond energy of about 941 kJ mol^{-1}.[6–11] One big issue for the NRR in aqueous electrolytes is that the competitive hydrogen evolution reaction (HER) limits its current efficiency and leads to a low overall reaction rate (Fig. 1).[12] Although they have better NH_3 selectivity, molecular catalysts are fragile, which can be circumvented by using heterogeneous NRR catalysts.

Two basic mechanisms (Scheme 1) are involved in the NRR over heterogeneous catalysts: the dissociative and associative mechanisms.[13] In the dissociative mechanism, the N≡N triple bond is broken before its hydrogenation, leaving individual N-adatoms on the catalyst surface which are transformed into NH_3 independently (Scheme 1a). The NRR based on the associative mechanism proceeds *via* an alternating (Scheme 1b) and a distal (Scheme 1c) pathway. For the alternating pathway, each

---

[a] *Institute of Fundamental and Frontier Sciences, University of Electronic Science and Technology of China, Chengdu 610054, Sichuan, China. E-mail: xpsun@uestc.edu.cn*
[b] *Chemical Synthesis and Pollution Control Key Laboratory of Sichuan Province, College of Chemistry and Chemical Engineering, China West Normal University, Nanchong 637002, Sichuan, China*
[c] *The Key Laboratory of Life-Organic Analysis, Key Laboratory of Pharmaceutical Intermediates and Analysis of Natural Medicine, School of Chemistry and Chemical Engineering, Qufu Normal University, Qufu 273165, Shandong, China*
[d] *School of Materials Science and Engineering, Henan Normal University, Xinxiang 453007, Henan, China*

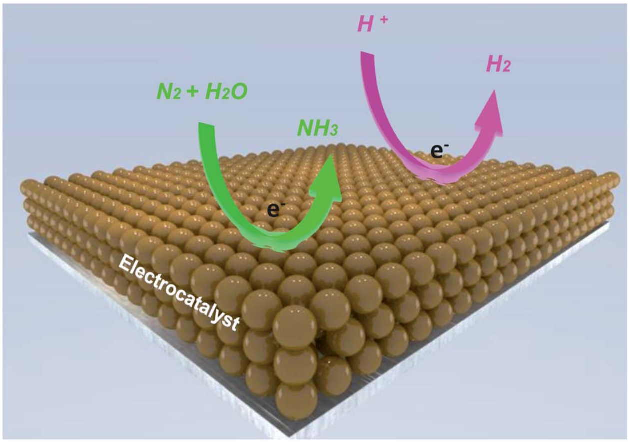

Fig. 1 Competition between the electrocatalytic NRR and HER processes on the catalyst. The NRR process involves the transfer of six electrons for one N_2 molecule: N_2 (g) + $6H_2O$ (l) + $6e^-$ $\leftrightharpoons$ $2NH_3$ (aq.) + $6OH^-$ (aq.) ($E^\circ = 0.092$ V *vs.* the reversible hydrogen electrode, RHE). In this process, N_2 reacts with protons from the electrolyte on the surface of the catalyst to form NH_3 using electrons from the electrode. Because of the involvement of only two electrons per H_2 molecule, $2H^+$ (aq.) + $2e^-$ $\leftrightharpoons$ H_2 (g) ($E^\circ = 0.00$ V *vs.* RHE), the HER is kinetically preferred over the multi-step six-electron NRR process.

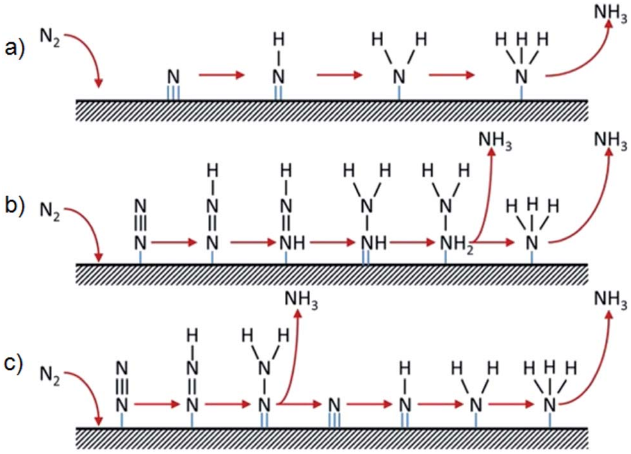

Scheme 1 Generic NRR mechanisms on heterogeneous catalysts: (a) dissociative pathway; (b) associative alternating pathway; and (c) associative distal pathway. Reproduced from ref. 13 with permission from Elsevier, copyright 2018.

of the two N atoms of adsorbed N_2 is hydrogenated in turn until one N atom is converted into NH_3 and the triple bond is broken. For the distal one, preferential hydrogenation of the N atom furthest away from the surface releases one equivalent of NH_3, followed by the hydrogenation of the other N-adatom to release a second equivalent of NH_3.

In this Minireview, we summarize the recent advances in developing NRR electrocatalysts including noble-metal, non-noble-metal and non-metal catalysts. Following this, we discuss the strategies to boost the NRR performances including electronic structure tailoring, active site enrichment and HER suppression. Finally, future research directions are also proposed in the concluding remarks.

2. Advances in NRR electrocatalysts

2.1. Noble-metal catalyst

Based on previous density functional theory (DFT) calculations predicting a stronger binding of intermediates to the stepped facets than to the flat terraces on a N_2-fixing metal catalyst,[14] Yan and co-workers demonstrated a proof-of-concept that a Au nanorod with a tetrahexahedral structure is capable of catalyzing the NRR with an NH_3 yield of 1.648 μg h^{-1} cm^{-2} and a faradaic efficiency (FE) of 4.02%.[15] Wang *et al.* reported that Pd/C is superior in NRR activity to Au and Pt in phosphate buffer solution (PBS), attaining a FE of 8.2%.[16] Theoretical calculations further reveal that the *in situ* formed α-PdH enables N_2 activation through a thermodynamically more favorable Grotthuss-like hydride transfer pathway compared to direct surface hydrogenation or proton-coupled electron transfer steps. Ru is industrially used as an alternative to conventional Fe catalysts for more efficient NH_3 synthesis at lower temperatures.[17] Recent work also shows that Ru nanoparticles perform efficiently in ambient electrocatalytic N_2 reduction to NH_3 (5.5 mg h^{-1} m^{-2}; 5.4%).[18] Of note, Ag nanosheets also provides quite positive results (4.8%).[19]

2.2. Non-noble-metal catalysts

Compared with noble-metal materials, non-noble-metal ones have much higher earth abundance and hence hold greater promise for application as attractive NRR catalysts. Biological nitrogenases containing Mo, Fe and V are involved in natural N_2 fixation,[20,21] and a variety of NRR electrocatalysts made of these metals have been developed for artificial electrochemical NH_3 synthesis under ambient conditions.

Inspired by the fact that Mo and S elements play significant roles in nitrogenases, we performed theoretical calculations to study the electronic structures of MoS_2 and mapped out the energy profile of the NRR on MoS_2, which suggests that the positively charged Mo-edge is the key to polarizing and activating the N_2 molecules (Fig. 2).[22] To prove this, we hydrothermally grew a MoS_2 nanosheet array on carbon cloth (MoS_2/CC) to catalyze the NRR with a FE of 1.17%. Interestingly, other Mo compounds are also active for the NRR. For instance, an MoN catalyst can suppress electron transfer from Mo to the adsorbed N_2, facilitating the release of produced NH_3 and thus enhancing the NRR performance, and MoN nanosheets achieve an NH_3 yield of 3.01×10^{-10} mo1 s^{-1} cm^{-2} with a FE of 1.15%.[23] Superior NRR performances have been reported for Mo_2C nanorods[24] and Mo_2C nanodots embedded in ultrathin carbon nanosheets[25] with FEs of 8.13% and 7.8%, respectively. The exposed Mo atoms of the $Mo_2C(121)$ surface have large adsorption energies to dissociate N_2 and the subsequent exothermic hydrogenation reactions are energetically preferable *via* the alternating pathway.[25] Compared with the above Mo-based catalysts, its oxide counterpart can be more easily prepared on a large scale, and our study also verifies that MoO_3

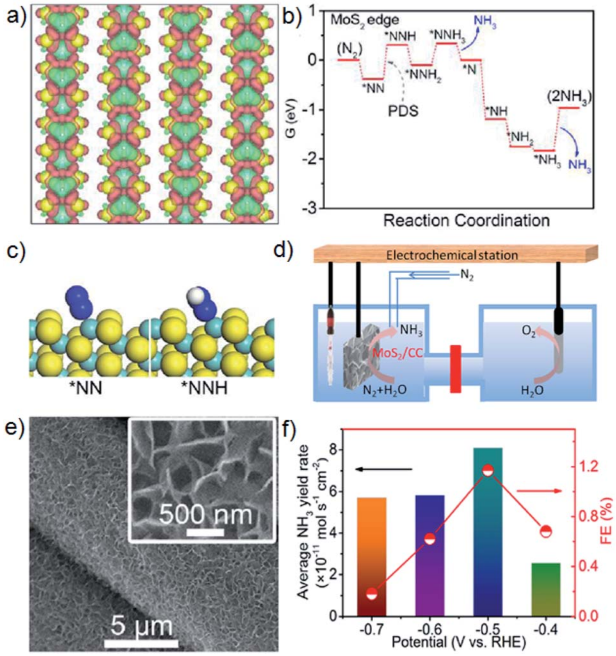

Fig. 2 (a) Isosurface of deformation charge density as viewed from the top. Red and green represent charge accumulation and loss, respectively. The isosurface is 0.0025 a.u. (b) Free energy profiles for the NRR at the MoS_2 edge site. The asterisk (*) denotes the adsorption site. (c) Structures of key intermediates of the potential-determining step (PDS). (d) A schematic diagram to illustrate the electrochemical setup for the NRR tests. (e) Scanning electron microscopy (SEM) images for MoS_2/CC. (f) Average NH_3 yields and FEs of MoS_2/CC at different potentials in 0.1 M Na_2SO_4. Reproduced from ref. 22 with permission from Wiley-VCH, copyright 2018.

nanosheets are active for electrocatalytic N_2-to-NH_3 fixation (4.80×10^{-10} mol s^{-1} cm^{-2}; 1.9%).[26]

As the cheapest and one of the most abundant transition metals, Fe-based NRR catalysts have also been widely explored. Licht *et al.* reported efficient N_2 reduction using Fe_2O_3 in a molten hydroxide electrolyte cell at temperatures ≥ 200 °C.[27] At room temperature and pressure, however, only a low FE of 0.15% was obtained for Fe_2O_3 nanoparticles supported on carbon nanotubes in a flow electrochemical cell operating in the gas phase.[28] Since then, much effort has been made to explore Fe oxides with higher NRR activities in aqueous media.[29–31] An Fe_3S_4 nanocatalyst was also shown by Zhao *et al.* to be active with a FE of 6.45% for NH_3 formation.[32] For the first time, we demonstrate that FeOOH nanorods achieve a FE of 6.7%, and DFT calculations evidence that the Fe-edge atom of the FeOOH(110) surface plays a key role in polarizing and activating the N_2 molecules for both charge exchange and transfer.[33] Quite surprisingly, a more recent study by us suggests that a P-rich FeP_2 nanoparticle-reduced graphene oxide hybrid exhibits superhigh performances with a large NH_3 yield of 35.26 μg h^{-1} mg$_{cat.}$$^{-1}$ and a high FE of 21.99%.[34] DFT calculations reveal decreased HER activity, higher N_2 adsorption energy, and a larger number of NRR active sites for FeP_2 compared to FeP.

VN has previously been identified by DFT analysis as a promising candidate for the NRR under ambient conditions,[35] but only recently has this prediction been experimentally verified.[36–38] For transition metal nitrides, a Mars-van Krevelen mechanism is considered for NH_3 generation: a surface N atom is reduced to form NH_3 after which the resulting vacancy is replenished by a N_2 molecule from the electrolyte. The N-vacancy must be stable at the surface, thus avoiding migration into the bulk of the catalyst. If not so, the reacted N on the surface is only replaced with more N atoms from the catalyst itself until all the N atoms of the metal nitrides are completely depleted, leaving only pure metal. V oxides are also able to catalyze the NRR.[39,40] It should be noted that many other metals without biological implications, including Ti,[41–43] Nb,[44,45] Cr,[46] Mn,[47] Co,[48] Cu,[49] Bi,[50,51] Sn,[52] La,[53] *etc.*, have also been identified to actively electrocatalyze the reduction.

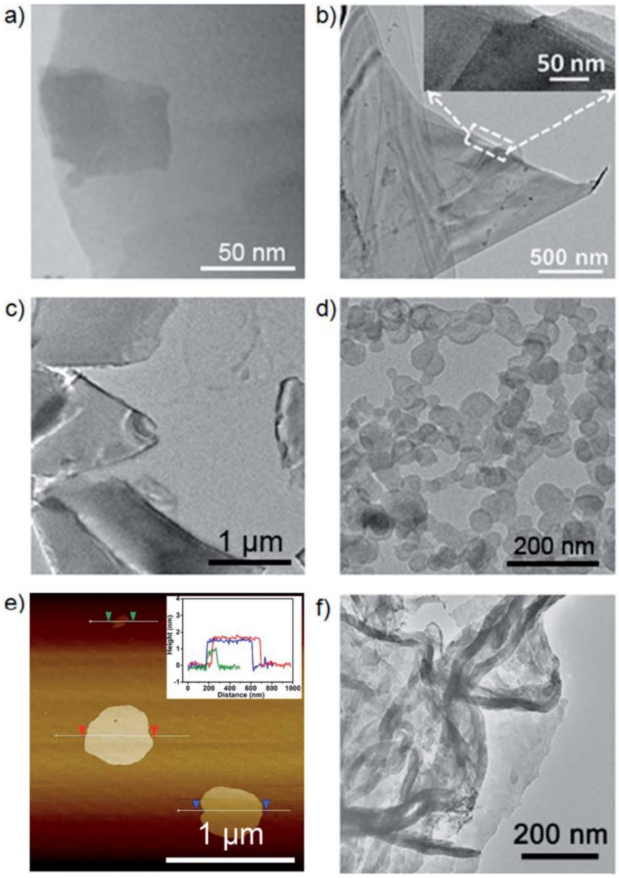

Fig. 3 Transmission electron microscopy (TEM) images of non-metal catalysts: (a) B nanosheet. Reproduced from ref. 56 with permission from The Royal Society of Chemistry, copyright 2019; (b) black P nanosheet. Reproduced from ref. 57 with permission from Wiley-VCH, copyright 2019; (c) B_4C nanosheet. Reproduced from ref. 58 with permission from the Nature Publishing Group, copyright 2018; (d) BP nanoparticles. Reproduced from ref. 59 with permission from The Royal Society of Chemistry, copyright 2019; (f) PCN. Reproduced from ref. 62 with permission from Wiley-VCH, copyright 2018; (e) atomic force microscopy image and corresponding height profile for BN nanosheets. Reproduced from ref. 61 with permission from Tsinghua University Press and Springer-Verlag, copyright 2019.

Table 1 Performance metrics of aqueous-based NRR electrocatalysts under ambient conditions

		Catalyst	Electrolyte	Potential (V) *vs.* RHE	NH_3 yield	FE (%)	Ref.
Catalyst development	Noble-metal catalysts	Au nanorods	0.10 M KOH	−0.2	1.648 μg h^{-1} cm^{-2}	4.02	*Adv. Mater.*, 2017, **29**, 1604799
		Pd/C	0.01 M HCl		4.5 μg h^{-1} $mg_{Pd}{}^{-1}$ (−0.05 V)	8.2 (0.1 V)	*Nat. Commun.*, 2018, **9**, 1795
		Ru nanoparticles	0.01 M HCl		5.5 μg h^{-1} cm^{-2} (−0.1 V)	5.4 (0.01 V)	*ChemSusChem*, 2018, **11**, 3416–3422
		Ag nanosheets	0.1 M HCl	−0.6	4.62×10^{-11} mol s^{-1} cm^{-2}	4.8	*Chem. Commun.*, 2018, **54**, 11427–11430
	Non-noble-metal catalysts	MoS_2 nanosheet array	0.1 M Na_2SO_4	−0.5	8.08×10^{-11} mol s^{-1} cm^{-1}	1.17	*Adv. Mater.*, 2018, **30**, 1800191
		MoN nanosheet array	0.1 M HCl	−0.3	3.01×10^{-10} mo1 s^{-1} cm^{-2}	1.15	*ACS Sustainable Chem. Eng.*, 2018, **6**, 9550–9554
		Mo_2C/C	0.5 M Li_2SO_4	−0.3	11.3 μg h^{-1} $mg_{Mo_2C}{}^{-1}$	7.8	*Adv. Mater.*, 2018, **30**, 1803694
		Mo_2C nanorods	0.1 M HCl	−0.3	91.5 μg h^{-1} $mg_{cat.}{}^{-1}$	8.31	*ACS Central Sci.*, 2019, **5**, 116–121
		MoO_3 nanosheets	0.1 M HCl		4.8×10^{-10} mol s^{-1} cm^{-2} (−0.5 V)	1.9 (−0.3 V)	*J. Mater. Chem. A*, 2018, **6**, 12974–12977
		Fe_2O_3-CNT	$KHCO_3$	−2.0	0.22 μg h^{-1} cm^{-2}	0.15	*Angew. Chem., Int. Ed.*, 2017, **56**, 2699–2703
	Non-noble-metal catalysts	Fe/Fe_3O_4	0.1 M PBS	−0.3	0.19 μg h^{-1} cm^{-2}	8.29	*ACS Catal.*, 2018, **8**, 9312–9319
		Fe_2O_3 nanorods	0.1 M Na_2SO_4	−0.8	15.9 μg h^{-1} mg^{-1}	0.94	*ChemCatChem*, 2018, **10**, 4530–4535
		Fe_3O_4 nanorods	0.1 M Na_2SO_4	−0.4	5.6×10^{-11} mol s^{-1} cm^{-2}	2.6	*Nanoscale*, 2018, **10**, 14386–14389
		β-FeOOH nanorods	0.5 M $LiClO_4$		23.32 μg h^{-1} $mg_{cat.}{}^{-1}$ (−0.75 V)	6.7 (−0.7 V)	*Chem. Commun.*, 2018, **54**, 11332–11335
		Fe_3S_4 nanosheets	0.1 M HCl	−0.4	75.4 μg h^{-1} $mg_{cat}{}^{-1}$	6.45	*Chem. Commun.*, 2018, **54**, 13010–13013
		VN nanoparticles	0.05 M H_2SO_4	−0.1	3.3×10^{-10} mol s^{-1} cm^{-2}	6.0	*J. Am. Chem. Soc.*, 2018, **140**, 13387–13391
		VN nanosheet array	0.1 M HCl	−0.5	8.4×10^{-11} mol s^{-1} cm^{-2}	2.25	*ACS Sustainable Chem. Eng.*, 2018, **6**, 9545–9549
		TiO_2 nanosheet array	0.1 M Na_2SO_4	−0.7	9.16×10^{-11} mol s^{-1} cm^{-2}	2.5	*ACS Appl. Mater. Interfaces*, 2018, **10**, 28251–28255
		$Ti_3C_2T_x$ nanosheets	0.1 M HCl	−0.4	20.4 μg h^{-1} $mg_{cat.}{}^{-1}$	9.3	*J. Mater. Chem. A*, 2018, **6**, 24031–24035
		$Ti_3C_2T_x$/FeOOH	0.05 M H_2SO_4		0.53 μg·h^{-1}·cm^{-2} (−0.5 V)	5.78 (−0.2 V)	*Joule*, 2019, **3**, 279–289
		NbO_2 nanoparticles	0.05 M H_2SO_4	−0.65	11.6 μg h^{-1} $mg_{cat.}{}^{-1}$	32	*Small Methods*, 2019, **3**, 1800386
		Nb_2O_5 nanofibers	0.1 M HCl	−0.55	43.6 μg h^{-1} $mg_{cat.}{}^{-1}$	9.26	*Nano Energy*, 2018, **52**, 264–270
		Hollow Cr_2O_3 microspheres	0.1 M Na_2SO_4	−0.9	25.3 μg h^{-1} $mg_{cat.}{}^{-1}$	6.78	*ACS Catal.*, 2018, **8**, 8540–8544
		MnO particles	0.1 M Na_2SO_4	−0.39	1.11×10^{-10} mol s^{-1} cm^{-2}	8.02	*Adv. Sci.*, 2019, **6**, 1801182
		LaF_3 nanoplates	0.5 M $LiClO_4$	−0.45	55.9 μg h^{-1} $mg_{cat.}{}^{-1}$	16.0	*J. Mater. Chem. A*, 2019, **7**, 17761–17765
		Mosaic Bi nanosheets	0.1 M Na_2SO_4	−0.8	2.54 ± 0.16 $μg_{NH_3}$ cm^{-2} h^{-1}	10.46 ± 1.45	*ACS Catal.*, 2019, **9**, 2902–2908
		Bi nanosheet array	0.1 M HCl	−0.5	6.89×10^{-11} mol s^{-1} cm^{-2}	10.26	*Chem. Commun.*, 2019, **55**, 5263–526
		CuO/rGO	0.1 M Na_2SO_4	−0.75	1.8×10^{-10} mol s^{-1} cm^{-2}	3.9%	*ChemCatChem*, 2019, **11**, 1441–1447
	Non-metal catalysts	B nanosheets	0.1 M HCl	−0.14	31.37 μg h^{-1} $mg_{cat.}{}^{-1}$	4.84	*Chem. Commun.*, 2019, **55**, 4246–4249
		B nanosheets	0.1 M Na_2SO_4	−0.8	13.22 μg h^{-1} $mg_{cat.}{}^{-1}$	4.04	*ACS Catal.*, 2019, **9**, 4609–4615
		Black P nanosheets	0.01 M HCl		31.37 μg h^{-1} $mg_{cat.}{}^{-1}$ (−0.7 V)	5.07 (−0.6 V)	*Angew. Chem., Int. Ed.*, 2019, **58**, 2612–2616
		B_4C nanosheets	0.1 M HCl	−0.75	26.57 μg h^{-1} $mg_{cat.}{}^{-1}$	15.95	*Nat. Commun.*, 2018, **9**, 3485
		BP nanoparticles	0.1 M HCl	−0.6	26.42 μg h^{-1} $mg_{cat.}{}^{-1}$	12.7	*J. Mater. Chem. A*, 2019, **7**, 16117–16121
		BN nanosheets	0.1 M HCl	−0.75	22.4 μg h^{-1} $mg_{cat.}{}^{-1}$	4.7	*Nano Res.*, 2019, **12**, 919–924
		Mesoporous BN	0.1 M Na_2SO_4	−0.7	18.2 μg h^{-1} $mg_{cat.}{}^{-1}$	5.5	*Nanoscale*, 2019, **11**, 4231–4235
		PCN	0.1 M HCl	−0.2	8.09 μg h^{-1} $mg_{cat.}{}^{-1}$	11.59	*Angew. Chem., Int. Ed.*, 2018, **57**, 10246–10250
Performance improvement	Tailoring electronic structures	Defective TiO_2	0.1 M HCl	−0.15	1.24×10^{-10} mol s^{-1} cm^{-2}	9.17	*Nanoscale*, 2019, **11**, 1555–1562
		MnO_x nanowire array	0.1 M Na_2SO_4	−0.5	1.63×10^{-10} mol s^{-1} cm^{-2}	11.40	*Chem. Commun.*, 2019, **55**, 4627–4630
		R-WO_3 nanosheets	0.1 M HCl	−0.3	17.28 μg h^{-1} $mg_{cat.}{}^{-1}$	7.0	*Nanoscale*, 2019, **11**, 19274–19277
		r-CeO_2 nanorods	0.1 M Na_2SO_4		16.4 μg h^{-1} $mg_{cat.}{}^{-1}$ (−0.5 V)	3.7 (−0.4 V)	*ACS Sustainable Chem. Eng.*, 2019, **7**, 2889–2893
		W_2N_3 nanosheets	0.1 M KOH	−0.2	11.66 ± 0.98 μg h^{-1} $mg_{cat.}{}^{-1}$	11.67 ± 0.93	*Adv. Mater.*, 2019, **31**, 1902709
		Defect-rich MoS_2 nanoflowers	0.1 M Na_2SO_4	−0.4	29.28 μg h^{-1} $mg_{cat.}{}^{-1}$	8.34	*Adv. Energy Mater.*, 2018, **8**, 1801357
		Defect-Bi nanoplates	0.2 M Na_2SO_4	−0.6	5.453 μg h^{-1} $mg_{Bi}{}^{-1}$	11.6	*Angew. Chem., Int. Ed.*, 2019, **58**, 9464–9469

Table 1 (*Contd.*)

	Catalyst	Electrolyte	Potential (V) *vs.* RHE	NH_3 yield	FE (%)	Ref.
	NPC	0.05 M H_2SO_4	−0.9	1.40 mmol g^{-1} h^{-1}	1.42	*ACS Catal.*, 2018, **8**, 1186–1191
	NCM-Au NPs	0.1 M KOH		0.36 g m^{-2} h^{-1} (−0.2 V)	22 (−0.1 V)	*Angew. Chem., Int. Ed.*, 2018, **57**, 12360–12364
	B-Doped graphene	0.05 M H_2SO_4	−0.5	9.8 μg h^{-1} cm^{-2}	10.8	*Joule*, 2018, **2**, 1610–1622
	O-Doped graphene	0.1 M HCl		21.3 μg h^{-1} $mg_{cat.}{}^{-1}$ (−0.55 V)	12.6 (−0.45 V)	*Chem. Commun.*, 2019, **55**, 7502–7505
	S-Doped graphene	0.1 M HCl		27.3 μg h^{-1} $mg_{cat.}{}^{-1}$ (−0.6 V)	11.5 (−0.5 V)	*Chem. Commun.*, 2019, **55**, 3371–3374
Tailoring electronic structures	Defect-rich fluorographene	0.1 M Na_2SO_4	−0.7	9.3 μg h^{-1} $mg_{cat.}{}^{-1}$	4.2	*Chem. Commun.*, 2019, **55**, 4266–4269
	FeO(OH,F) nanorods	0.5 M $LiClO_4$	−0.6	42.38 μg h^{-1} $mg_{cat.}{}^{-1}$	9.02	*Chem. Commun.*, 2019, **55**, 3987–3990
	F-SnO_2 nanosheets	0.1 M Na_2SO_4	−0.45	19.3 μg h^{-1} $mg_{cat.}{}^{-1}$	8.6	*Inorg. Chem.*, 2019, **58**, 10424–10431
	Cu-CeO_{2-x} nanorods	0.1 M Na_2SO_4	−0.45	5.3 × 10^{-10} mol s^{-1} cm^{-2}	19.1	*Chem. Commun.*, 2019, **55**, 2952–2955
	C-Ti_xO_y/C	0.1 M $LiClO_4$	−0.4	14.8 μg h^{-1} $mg_{cat.}{}^{-1}$	17.8	*Angew. Chem., Int. Ed.*, 2019, **58**, 13101–13106
	V-TiO_2 nanorods	0.5 M $LiClO_4$		17.73 μg h^{-1} $mg_{cat.}{}^{-1}$ (−0.5 V)	15.3 (−0.4 V)	*Small Methods*, 2019, **3**, 1900356
	Zr-TiO_2 nanotubes	0.1 M KOH	−0.45	8.90 μg h^{-1} cm^{-2}	17.3	*Nat. Commun.*, 2019, **10**, 2877
	Fe-TiO_2 nanoparticles	0.5 M $LiClO_4$	−0.4	25.47 μg h^{-1} $mg_{cat.}{}^{-1}$	25.6	*Angew. Chem., Int. Ed.*, 2019, **131**, 18620–18624
	O-CNT	0.1 M $LiClO_4$	−0.4	32.33 μg h^{-1} $mg_{cat.}{}^{-1}$	12.50	*Chem. Commun.*, 2019, **55**, 4997–5000
	TA-rGO	0.5 M $LiClO_4$	−0.75	17.02 μg h^{-1} $mg_{cat.}{}^{-1}$	4.83	*ACS Sustainable Chem. Eng.*, 2019, **7**, 14368−14372
	Pd-TA	0.1 M Na_2SO_4	−0.45	24.12 μg h^{-1} $mg_{cat.}{}^{-1}$	9.4	*J. Mater. Chem. A*, 2019, **7**, 21674–21677
	a-Au/CeO_x-rGO	0.1 M HCl	−0.2	8.31 μg h^{-1} $mg_{cat.}{}^{-1}$	10.10	*Adv. Mater.*, 2017, **29**, 1700001
	$Bi_4V_2O_{11}$/CeO_2	0.1 M HCl	−0.2	23.21 μg h^{-1} $mg_{cat.}{}^{-1}$	10.16	*Angew. Chem., Int. Ed.*, 2018, **57**, 6073–6073
	Au_6/Ni	0.05 M H_2SO_4	−0.14	7.4 μg h^{-1} $mg_{cat.}{}^{-1}$	67.8	*J. Am. Chem. Soc.*, 2019, **141**, 14976–14980
Enriching active sites	TA-reduced Au/TiO_2	0.1 M HCl	−0.2	21.4 μg h^{-1} $mg_{cat.}{}^{-1}$	8.11	*Adv. Mater.*, 2017, **29**, 1606550
	Au flowers	0.1 M HCl	−0.2	25.57 μg h^{-1} $mg_{cat.}{}^{-1}$	6.05	*ChemSusChem*, 2018, **11**, 3480−3485
	AuHNCs	0.5 M $LiClO_4$		3.9 μg h^{-1} cm^{-2} (−0.5 V)	30.2 (−0.4 V)	*Nano Energy*, 2018, **49**, 316−323
	TiO_2-rGO	0.1 M Na_2SO_4	−0.9	15.13 μg h^{-1} $mg_{cat.}{}^{-1}$	3.3	*J. Mater. Chem. A*, 2018, **6**, 17303–17306
	Mn_3O_4-rGO	0.1 M Na_2SO_4	−0.85	17.4 μg h^{-1} $mg_{cat.}{}^{-1}$	3.52	*Nano Res.*, 2019, **12**, 1093–1098
	Cr_2O_3-rGO	0.1 M HCl		33.3 μg h^{-1} $mg_{cat.}{}^{-1}$ (−0.7 V)	7.33 (−0.6 V)	*Inorg. Chem.*, 2019, **58**, 2257–2260
	SnO_2/rGO	0.1 M Na_2SO_4	−0.5	25.6 μg h^{-1} $mg_{cat.}{}^{-1}$	7.1	*ACS Appl. Mater. Interfaces*, 2019, **11**, 31806–31815
	$Pd_{0.2}Cu_{0.8}$-rGO	0.1 M KOH	−0.7	2.8 μg h^{-1} $mg_{cat.}{}^{-1}$	0.6	*Adv. Energy Mater.*, 2018, **8**, 1800124
	S dots-rGO	0.5 M $LiClO_4$	−0.85	28.56 μg h^{-1} $mg_{cat.}{}^{-1}$	7.07	*Chem. Commun.*, 2019, **55**, 3152–3155
	PTCA-rGO	0.1 M HCl	−0.5	24.7 μg h^{-1} $mg_{cat.}{}^{-1}$	6.9	*J. Mater. Chem. A*, 2019, **7**, 12446–12450
	MnO_2–$Ti_3C_2T_x$	0.1 M HCl	−0.55	34.12 μg h^{-1} $mg_{cat.}{}^{-1}$	11.39	*J. Mater. Chem. A*, 2019, **7**, 18 823–18 827
	TiO_2/$Ti_3C_2T_x$	0.1 M HCl		32.17 μg h^{-1} $mg_{cat.}{}^{-1}$ (−0.55 V)	16.07 (−0.45 V)	*Adv. Energy Mater.*, 2019, **9**, 1803406
	BP/SnO_{2-x} nanotubes	0.1 M Na_2SO_4	−0.4	48.87 μg h^{-1} $mg_{cat.}{}^{-1}$	14.6	*Angew. Chem., Int. Ed.*, 2019, **131**, 1–7
	Au_1/C_3N_4	0.05 M H_2SO_4	−0.1	1.305 μg h^{-1} $mg_{Au}{}^{-1}$	11.1	*Sci. Bull.*, 2018, **63**, 1246−1253
	AuSAs-NDPCs	0.1 M HCl	−0.2	2.32 μg h^{-1} cm^{-2}	12.3	*Small Methods*, 2018, **2**, 1800202
	Ru SAs/N–C	0.05 M H_2SO_4	−0.2	120.9 μg h^{-1} $mg_{cat.}{}^{-1}$	29.6	*Adv. Mater.*, 2018, **30**, 1803498
	SA-Mo/NPC	0.1 M KOH	−0.3	34.0 ± 3.6 μg h^{-1} $mg_{cat.}{}^{-1}$	14.6 ± 1.6	*Angew. Chem., Int. Ed.*, 2019, **58**, 2321–2325
Enriching active sites	FeSA-N–C	0.1 M KOH	0.0	7.48 μg h^{-1} $mg_{cat.}{}^{-1}$	56.55	*Nat. Commun.*, 2019, **10**, 341
	PEBCD	0.5 M Li_2SO_4		2.01 μg h^{-1} cm^{-2} (−0.7 V)	2.91 (−0.4 V)	*J. Am. Chem. Soc.*, 2017, **139**, 9771–9774
	MoS_2/BCCF	0.1 M Li_2SO_4	−0.2	43.4 μg h^{-1} $mg_{cat.}{}^{-1}$	9.81	*Adv. Energy Mater.*, 2019, **9**, 1803935
	BiNCs	Acidic 0.5 M K_2SO_4 (pH = 3.5)	−0.6	200 mmol g^{-1} h^{-1}	66	*Nat. Catal.*, 2019, **2**, 448–456
	Ag-Au@ZIF	0.1 M HCl	−2.5	10 pmol cm^{-2} s^{-1}	18 ± 4	*Sci. Adv.*, 2018, **4**, eaar3208
	NPG@ZIF-8	0.1 M Na_2SO_4		28.7 ± 0.9 μg h^{-1} cm^{-2} (−0.8 V)	44 (−0.6 V)	*Angew. Chem., Int. Ed.*, 2019, **131**, 15506−15510

2.3. Non-metal catalysts

From economic and environmental viewpoints, using non-metal catalysts could lower the cost and avoid the residues of metal ions. Nanocarbons, which are mainly composed of carbon and can even be made directly out of biomass, feature wide potential windows and structural diversity, which make them promising for electrochemical application as sustainable materials.[54] Unfortunately, pristine nanocarbons have poor NRR activities and effective strategies must be implemented to improve their catalytic performances (see the following section for details).

Interestingly, nanomaterials of elemental B[55,56] and black P[57] perform efficiently in electrochemical NH_3 synthesis. Other non-metal materials including B_4C,[58] BP,[59] BN,[60,61] and polymeric carbon nitride (PCN)[62] are highly active NRR catalysts. Fig. 3 presents the morphologies and the performance metrics are detailed in Table 1.

3. Strategies for boosting the NRR performances

The catalytic performances of current catalysts are still far from meeting the needs of practical applications. From the point of view of thermodynamics, the NRR should proceed at negative potentials that are dominated by the competing HER, leading to a tough selectivity issue and thus unsatisfactory current efficiency. It is clear that strategies should be developed to enable more efficient N_2 reduction electrocatalysis. In the following section, we will summarize the most recent progress in strategies to boost the NRR performances, which include: (1) tailoring the electronic structures to promote intrinsic NRR activity; (2) enriching active sites to increase the apparent NRR activity; (3) suppressing the HER to improve the selectivity.

3.1. Tailoring the electronic structures of catalysts

Tailoring the electronic structure of a catalyst is the most common method to change the adsorption behaviour and tune the intrinsic activity of each active site.[63] Defect engineering and heteroatom doping have been proven to be the two most effective methods to boost the intrinsic activity of NRR electrocatalysts. Surface functionalization and interface engineering provide us with two other good choices for this purpose.

3.1.1 Defect engineering. O vacancies (V_O) can manipulate the electronic structure of metal oxides to achieve enhanced conductivity and could also act as the active sites to adsorb the reactants and reaction intermediates leading to a lowered activation energy barrier.[64] Li *et al.* reported that V_O in amorphous TiO_2 promote the adsorption and activation of N_2 facilitating N_2 photoreduction to NH_3.[65] Recently, we found that a TiO_2 nanosheet array can electrocatalyze the NRR with a FE of 2.50% in Na_2SO_4, and the *in situ* generated V_O during the NRR are supposed to be responsible for the enhanced adsorption and activation of N_2.[41] To gain further experimental and theoretical support for this, V_O were intentionally introduced into TiO_2 *via* cathodic polarization, and the resulting defective TiO_2 achieves a much higher FE (9.17%) than the pristine one (0.95%) in acid.[66] Such an enhancement is also observed for other metal oxides like MnO_2,[67] WO_3,[68] Fe_2O_3 (ref. 69) and CeO_2.[70]

The Yu group reported experimentally and theoretically that electrochemical N_2 reduction can be achieved by using PCN with N vacancies (V_N) which chemisorbs and significantly increases the bond length of N_2 resulting in strong N_2 activation.[62] Because of the lack of $^{15}N_2$ isotopic experiments, one cannot confirm that the N of NH_3 only comes from the N_2 feed gas. A more recent study by the Qiao group shows that V_N confined on 2D W_2N_3 nanosheets provide an electron-deficient environment to facilitate N_2 adsorption and lower the thermodynamic limiting potential of the NRR.[71] A nuclear magnetic resonance (NMR) test using $^{15}N_2$ as the feed gas verifies that the NH_3 was indeed generated *via* the NRR instead of decomposition of the catalyst or other contaminants.

The intrinsic high HER activity of MoS_2 limits its current efficiency for NH_3 formation.[22,72] We have addressed this issue by designing S-rich defective MoS_2 nanoflowers.[73] This catalyst attains a much higher FE of 8.34% than its defect-free counterpart (2.18%). The DFT results suggest that the defects lead to the d-band center of Mo atoms moving close to the Fermi level (-0.26 eV → -0.14 eV) related to a stronger interaction between the catalyst surface and N_2 molecule (-0.65 eV). Moreover, the defective MoS_2 has a lower energy barrier of the PDS (0.60 eV) than the pristine one (0.65 eV).

For pure metal catalysts, the defect effect is rarely studied. A recent study by the Yan group demonstrates the modulation of the electronic properties of Bi *via* defect engineering (Fig. 4).[74] In their study, Bi(110) nanoplates with a high fraction of isolated Bi vacancies were fabricated from Bi_2O_3 nanoplates using a low-temperature plasma bombardment approach. This defect-Bi achieves an NH_3 yield of 5.453 $\mu g\ h^{-1}\ mg_{cat.}^{-1}$ and a FE of 11.68%. Theoretical calculations indicate that defect-Bi(110) has a much lower activation energy (0.56 eV) in comparison with perfect-Bi(110) (1.03 eV) for the rate-determining step.

3.1.2 Heteroatom doping. Chemical doping with heteroatoms has also been proven to be an effective strategy to improve the electrocatalytic NRR activity. In Liu's study, N-doped porous carbon with a high N content and tunable N species was derived from zeolite imidazole framework-8 (ZIF-8) pyrolysis and tested for the NRR leading to an NH_3 yield of 23.8 $\mu g\ h^{-1}\ mg_{cat.}^{-1}$ and a FE of 1.42%.[75] Although the authors established the correlation between the level of N doping and the NRR performance based on their experimental and theoretical data, a persuasive conclusion is still pending because of the unavailability of $^{15}N_2$ isotopic experiment results. Wang *et al.* directly utilized a hierarchically structured N-doped nanoporous carbon membrane (NCM) as the working electrode for electrochemical N_2-to-NH_3 conversion with a FE of 5.2% and an NH_3 yield of 0.08 $g\ m^{-2}\ h^{-1}$.[76] Decorating this NCM electrode with Au nanoparticles further improves the performance metrics to 22% and 0.36 $g\ m^{-2}\ h^{-1}$, respectively.

As a 2D nanocarbon with high conductivity and chemical stability, graphene with B doping attains an NH_3 yield of 9.8 $\mu g\ h^{-1}\ cm^{-2}$ and a FE of 10.8%.[77] B incorporation causes redistribution of electron density and the as-formed electron-deficient B sites have higher N_2-binding capability. The much

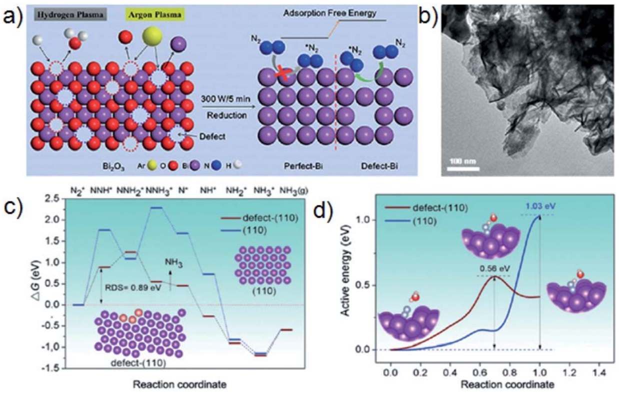

Fig. 4 (a) Illustration of the synthesis of a defect-Bi nanoplate and its application for the NRR; (b) TEM image of defect-Bi nanoplates; (c) free–energy diagrams for the NRR on the perfect-Bi(110) and defect-Bi(110) facets *via* a reaction pathway; (d) activation energy of the rate-determining step. Reproduced from ref. 74 with permission from Wiley-VCH, copyright 2019.

larger electronegativity of O with respect to C endows it with a stronger ability to manipulate the electronic properties of carbon catalysts. O-doped graphene derived from sodium gluconate was also identified by us as a superior NRR catalyst with a larger NH_3 yield of 21.3 μg h^{-1} mg$_{\text{cat.}}^{-1}$ and a higher FE of 12.6%.[78] DFT data show that both C═O and O–C═O groups make a greater contribution to the NRR than the C–O group. Other heteroatoms like S[79] and F[80] also work effectively as dopants to boost the NRR performances of graphene.

Like carbon materials, metal-based catalysts can also be doped with non-metal and metal heteroatoms to boost the NRR performances. F was utilized by us to dope FeOOH to decrease the reaction energy barrier, and the performance metrics are greatly boosted from 10.01 μg h^{-1} mg$_{\text{cat.}}^{-1}$ and 2.16% to 42.38 μg h^{-1} mg$_{\text{cat.}}^{-1}$ and 9.02%, respectively.[81] The same idea was followed by Liu *et al.* for SnO_2 mesoporous nanosheets,[82] and it could also be applicable to other metal oxides. Cu doping in CeO_2 was reported to form multiple V_O for dramatically enhanced catalytic activities.[83] For such a strategy, TiO_2 is the most extensively studied metal oxide and several dopants like C,[84,85] B,[86] V,[87] and Zr[88] work effectively. The C-doped TiO_2/C material derived from MIL-125(Ti) affords a high FE of 17.8%, which is attributed to the doping of C atoms into V_O and the formation of Ti–C bonds, which enable energetically more favourable N_2 activation.[85] In Zheng's work, given that Zr^{4+} has a similar d-electron configuration and oxide structure but relatively larger ionic size, it was doped into TiO_2 to induce the formation of adjacent bi-Ti^{3+} pairs as the most active centers for efficient N_2 lying-down chemisorption and activation (8.90 μg h^{-1} mg$_{\text{cat.}}^{-1}$; 17.3%) (Fig. 5).[88] Impressively, high-performance NRR catalysis can also be enabled over TiO_2 using Fe as a dopant due to the synergistic effect of bi-Ti^{3+} and V_O (25.47 μg h^{-1} mg$_{\text{cat.}}^{-1}$; 25.6%).[89]

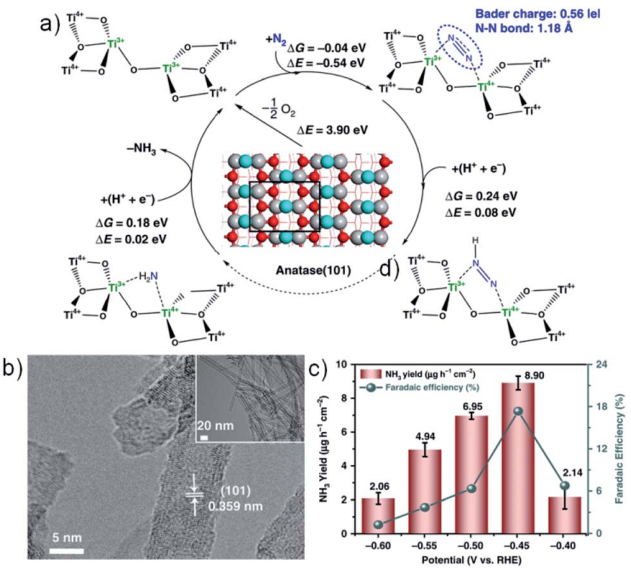

Fig. 5 (a) DFT prediction of the NRR activity for adjacent bi-Ti^{3+} on anatase (101) with V_O (light-blue spheres: lattice oxygen at the bridge sites where the surface V_O are formed most easily; red spheres: other lattice oxygens on the surfaces; gray spheres: titanium cations; ΔG: free energy; ΔE: electronic energy. (b) TEM image for Zr–TiO_2 nanotubes. (c) NH_3 yields and FEs of Zr–TiO_2 at each given potential. Reproduced from ref. 88 with permission from the Nature Publishing Group, copyright 2019.

3.1.3 Surface functionalization and interface engineering. To avoid using high-temperature thermal annealing to prepare carbon-based NRR catalysts, carbon nanotubes were acidically oxidized to introduce functional groups (C–O, OH, COOH, C═O) on their surface, and as a NRR catalyst, they exhibit superior performances (32.33 μg h^{-1} mg$_{\text{cat.}}^{-1}$; 12.50%).[90] Our recent work further shows an enhancement in the NRR activity of reduced graphene oxide (rGO) after surface modification with oxygen-rich tannic acid (TA).[91] The strong π–π stacking interactions between π-rich TA and rGO brings TA into very close proximity with rGO, which leads to intimate contact between the oxygen functional groups of TA and rGO favouring more effective manipulation of its electronic properties. The same strategy has also been used to improve the NRR performances of Pd catalysts (24.12 μg h^{-1} mg$_{\text{cat.}}^{-1}$; 9.49%).[92] Compared to Pd, the much larger electronegativity of the O of TA could drive the formation of electron-deficient Pd with enhanced N_2-adsorption ability,[69] but the exact enhancement mechanism is not completely understood at the present time.

Because amorphous catalysts are in a metastable state with abundant unsaturated coordination sites, they exhibit higher catalytic activity than the crystalline ones. To this end, Shi *et al.* achieved the amorphization of Au nanoparticles anchored on rGO using CeO_x as a trigger, and the resulting a-Au/CeO_x-rGO hybrid shows superior NRR performances (8.31 μg h^{-1} mg$_{\text{cat.}}^{-1}$; 10.10%) to other control catalysts.[93] The Yu group also reported highly active NRR electrocatalysis enabled by a CeO_2/amorphous $Bi_4V_2O_{11}$ hybrid (23.21 μg h^{-1} mg$_{\text{cat.}}^{-1}$; 10.16%).[94] The amorphous phase has more abundant defective sites and lowers the energy barrier, and CeO_2 triggers its amorphization during calcination. More recently, metal/metal interface engineering has also been applied to boost NRR catalysis, and the donor–

acceptor couple of Ni and Au nanoparticles with a strong electronic connection attains a superhigh FE of 67.8%.[95] In this study, Au nanoparticles were directly deposited on Ni nanoparticles *via* Galvanic replacement, and the electron-rich Au nanoparticles accepting electrons from Ni nanoparticles facilitate the adsorption and activation of N_2 molecules.

3.2. Enriching the active sites of catalysts

Enriching the active sites to increase the apparent activity is regarded as the most straightforward way to boost the catalytic performances of electrocatalysts. To obtain a more active catalyst, one promising approach is nanostructuring of the catalyst to significantly increase the number of active sites. Previous studies point out that the size and shape of catalysts have a large influence on their NRR activities. The Yan group reported using Au sub-nanoclusters on TiO_2 as a more efficient catalyst (21.4 μg h^{-1} cm^{-2}; 8.11%) due to the fact that the small size of the sub-nanoclusters with high surface energy facilitates the formation of strong Au–O–Ti bonds and the resulting positively charged Au centers favour N_2 adsorption.[96] Au flowers were also reported to show higher performances than Au spheres, which is attributed to the exposure of more active sites by the dendritic structures of Au flowers.[97] Using hollow gold nanocages as a NRR catalyst, Nazemi *et al.* attained a FE of 30.2% with an NH_3 yield of 3.9 μg h^{-1} cm^{-2}.[98] Such a unique hollow nanostructure not only exposes abundant active sites, but also provides a confined reaction environment that increases the residence time of N_2 molecules on its inner surface to enhance the conversion of N_2 to NH_3. In another study, we analyzed the performances of Cr_2O_3 catalysts, including hollow microspheres, solid microspheres, and nanoparticles with the following performance metrics: 25.3 μg h^{-1} $mg_{cat.}^{-1}$ & 6.78%, 11.4 μg h^{-1} $mg_{cat.}^{-1}$ & 2.94%, and 13.8 μg h^{-1} $mg_{cat.}^{-1}$ & 4.73%.[46]

Another attractive approach is to disperse electrocatalysts on supports with a high surface area and conductivity. Using such a support can better disperse and reduce aggregation of the nanocatalysts on one hand and enhance the charge transport on the other hand. Thus far, graphene has been largely used to support CoO,[48] CuO,[49] Au/CeO_x,[93] TiO_2,[99] Mn_3O_4,[100] Cr_2O_3,[101] SnO_2,[102] Fe_2O_3,[103] FeOOH,[104] PdCu,[105] PdP_2,[106] Ru_2P,[107] S dots,[108] and perylene-3,4,9,10-tetracarboxylic acid nanorods.[109] Graphene is electrocatalytically inert for the NRR, and its use as an inactive support would thus have an adverse effect on NH_3 yield per unit mass. The high conductivity and large surface area of 2D $Ti_3C_2T_x$ MXene,[110] together with its intrinsic NRR activity,[43,111] are promising for its use as an ideal support for NRR catalysts. We grew whisker-like MnO_2 on $Ti_3C_2T_x$ flakes and the MnO_2–$Ti_3C_2T_x$ hybrid attains a large NH_3 yield of 34.12 μg h^{-1} $mg_{cat.}^{-1}$ and a high FE of 11.39%, superior to those of each component due to the synergistic catalytic effect.[112] In another study, Ti_3C_2Tx MXene nanosheets act as both the support and Ti source for *in situ* solvothermal development of V_O-rich TiO_2 nanoparticles, and this hybrid efficiently catalyzes the NRR (32.17 μg h^{-1} $mg_{cat.}^{-1}$; 16.07%).[113] More recently, black P quantum dots were stably confined on electrochemically active, electrically conductive black SnO_{2-x} nanotubes *via* Sn–P coordination, and both components in the hybrid synergistically catalyze the NRR to afford amazing performance metrics (48.87 μg h^{-1} $mg_{cat.}^{-1}$; 14.6%).[114]

Single-atom catalysts (SACs) with maximum atom-utilization efficiency and unique properties enable reasonable use of metal resources and achieve atom economy, and they have recently emerged as a new Frontier in materials and catalysis sciences. Encouragingly, the establishment of reliable synthetic strategies to guarantee the stabilization of single metal atoms against migration and agglomeration has aroused huge recent interest in exploring their electrocatalytic applications.[115] Several recent studies have described highly active N_2 reduction electrocatalysis enabled by SACs. Wang *et al.* synthesized atomically dispersed Au catalysts on carbon nitride for the NRR with a FE of 11.1% and an NH_3 yield of 1.305 μg h^{-1} mg_{Au}^{-1}, which is ~22.5 times as high as that for supported Au nanoparticles.[116] Au single sites stabilized on N-doped porous and highly oxidized carbon also enable efficient N_2 electroreduction (2.32 μg h^{-1} cm^{-2}; 12.3%).[117] An NH_3 yield of 120.9 μg h^{-1} $mg_{cat.}^{-1}$ was reported by Geng *et al.* over single Ru atoms anchored on N-doped carbon (Ru SAs/N–C).[118] Han *et al.* prepared single Mo atoms anchored to N-doped porous carbon, and the high-density active sites and hierarchically porous carbon frameworks led to an NH_3 yield of 34.0 ± 3.6 μg h^{-1} $mg_{cat.}^{-1}$ and a FE of 14.6 ± 1.6%.[119] Another recent study by Wang *et al.* confirms that single-atom Fe on N-doped carbon achieves a much lower NH_3 yield of 7.48 μg h^{-1} $mg_{cat.}^{-1}$ than Ru and Mo-based SACs.[120] These studies would open up an exciting new avenue to explore using SACs for electrocatalytic N_2 reduction, but care should be taken regarding these and other N-containing catalysts because they may decompose and leach N leading to inaccurate results.

3.3. Suppressing the HER

Suppressing the HER at the catalyst/electrolyte interface by manipulating the availability of H^+ is an attractive route to improving NRR selectivity. DFT calculations predict that polyimide has intrinsic sluggish HER activity with a large activation barrier and Li^+ association can further reduce the active sites to passivate the HER.[121] Inspired by this, Chen *et al.* reported a Li^+-incorporated poly(*N*-ethyl-benzene-1,2,4,5-tetracarboxylicdiimide) (PEBCD) to boost NRR selectivity, and the NRR and HER processes are effectively promoted and retarded, respectively, by associating Li^+ ions with the O atoms in the PEBCD matrix.[122] Although it achieves significant HER passivation, this catalyst attains a FE of only 2.85%, which could be due to its intrinsic low NRR activity. In another study by the Zhao group, in-operando created strong Li–S interactions endow S-rich MoS_2 with superior NRR activity (43.4 μg h^{-1} $mg_{cat.}^{-1}$; 9.81%).[123] Such interactions suppress the HER, facilitate N_2 adsorption and increase NRR activity.

Hao *et al.* recently reported a strategy to simultaneously promote NRR selectivity and activity using Bi nanocrystals and K^+ cations (Fig. 6).[124] The K^+ cations not only stabilize the key nitrogen-reduction intermediates but also regulate proton transfer to increase the selectivity. A previous study suggests

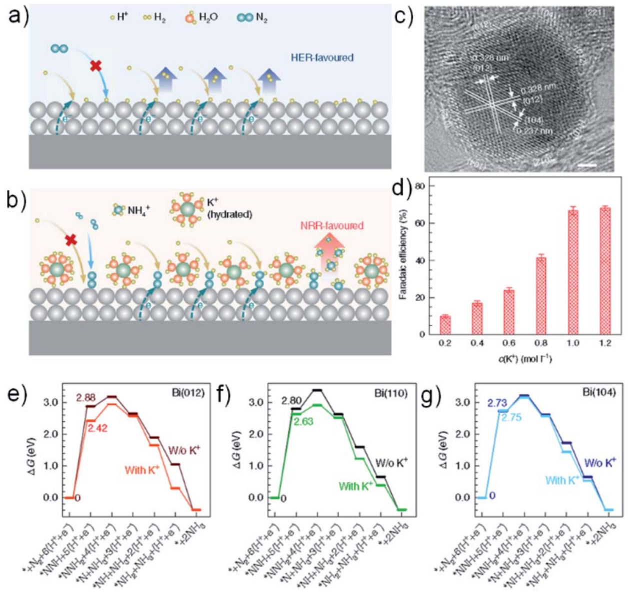

Fig. 6 Mass transfer of H^+ and N_2 to the catalyst surface in electrolytes (a) without and (b) with K^+. (a) In acidic solutions without K^+, H^+ can be transferred to the surface readily, and the HER will dominate. (b), K^+ hinders H^+ transfer to the catalyst surface. N_2 will be adsorbed preferentially, and the NRR is promoted. (c) High-resolution TEM image of BiNCs, showing the exposed surfaces of {012}, {104} and {110}. (d) FE *vs.* $c(K^+)$. Gibbs free–energy diagrams for the NRR on (e) Bi(012), (f) Bi(110), and (g) Bi(104) facets in the presence or absence of K^+ (pH 0 and $U = 0$ V *vs.* SHE). Reproduced from ref. 124 with permission from the Nature Publishing Group, copyright 2019.

that supporting cations with high concentration can retard H^+ migration from the bulk solution to the electrode surface leading to significant HER suppression.[125] In Hao's work, optimized NRR performances (200 mmol g^{-1} h^{-1}; 66%) were obtained in acidic 0.5 M K_2SO_4 electrolytes (pH = 3.5). Of note, such NRR promotion and HER suppression by K^+ can also apply to Au and Pt catalysts.

Coating a porous hydrophobic nanolayer over a NRR catalyst to repel water molecules could be another attractive alternative. This concept was first demonstrated in Ling's work.[12] The authors deposited Ag nanocubes onto an Au electrode, followed by coating with a bifunctional ZIF-71 thin film as a sorption layer for confining N_2 molecules to improve reactant–catalyst interactions and as a superhydrophobic barrier to inhibit water access. This structure affords a FE of 18 ± 4%, which is boosted by 10% compared to that of the uncoated catalyst. However, this system is neither cost-effective nor environmentally friendly because of the use of tetrahydrofuran and ethanol as the medium and proton source, respectively. An improved catalyst was recently designed by Yang *et al.*[126] In their work, nanoporous gold (NPG) as the core was coated with a ZIF-8 shell which weakens hydrogen evolution and retards reactant diffusion, leading to a superb aqueous-based NPG@ZIF-8 catalyst (28.7 ± 0.9 μg h^{-1} cm^{-2}; 44%). However, the authors have not commented on why the hydrophobic ZIF-8 can operate efficiently in an aqueous electrolyte.

The higher barrier for mass- and charge-transfer of neutral electrolytes leads to less favourable HER kinetics.[127] Wang *et al.* tested a Pd/C catalyst in PBS with a FE of 8.2%, but this catalyst only affords a FE lower than 0.1% in both H_2SO_4 and NaOH.[16] It is argued that PBS is a promising electrolyte for the electrochemical NRR due to its effective suppression of HER activity. Given the wide variety of experimental parameters tested in each study, this conclusion should be taken with caution because the large amount of research experience of our group suggests that the choice of electrolyte for optimized NRR performances also relies strongly on the catalyst itself.

4. Conclusions and outlook

The electrocatalysis community has made some recent progress in the design and development of catalytic systems to enable efficient electrochemical N_2 reduction to NH_3 under ambient conditions. An ideal catalyst should effectively adsorb and activate N_2 molecules to overcome the slow kinetics. By manipulating the electronic structures of NRR catalysts, we can promote their intrinsic activities. Increasing the number of exposed active sites provides us with the most straightforward way to enhance the apparent catalytic activity. As the HER has lower overpotentials, the NRR in aqueous electrolytes always suffers from strong HER competition, leading to limited selectivity for NH_3 formation. Despite some successful examples demonstrating the effective suppression of the HER to boost NRR selectivity, the versatility of this strategy has not been fully exploited. New strategies for catalyst design and HER suppression are still needed. Obviously, the selectivity issue will be better addressed by more general HER-retarding strategies like adding organic additives in the electrolytes or modifying the catalyst surface with water solvable H^+-repelling molecules. We shoud point out that it is not appropriate to only emphasize current efficiency, and NH_3 yield should also be treated seriously as an important metric for evaluating the overall performances of a NRR catalyst.

Recently, the reliability of the NRR results has provoked discussions of experimental protocols,[128] and strict standards have been set to obtain correct scientific reports.[129] Control measurements with Ar under the exact same conditions and with N_2 at open circuit potential are required to probe NH_3 contamination within the cell, catalyst, and feed gas.[130] Possible contaminants like NO_x and other labile nitrogen compounds can be effectively removed through adsorption on a reduced Cu catalyst,[129] and possible NH_3 and NO_x impurities can also be removed through a saturator filled with 0.05 M H_2SO_4 (aq.)[130] Provided that all these protocols are carefully taken into consideration,[129–131] both isotope-specific nuclear magnetic resonance and colorimetric measurements should give similar quantified results.[129] As a well-established technique for ion analysis, ion chromatography (IC) also provides quantitative results which are consistent with those of colorimetry.[47,66,80] Both colorimetry and IC measurements should also be considered as reliable alternatives to quantitatively gauge the NH_3 product. The future development of electrochemical NH_3 synthesis will heavily rely on establishing more efficient catalytic systems to achieve high selectivity and large current density for massive NH_3 production, which however will still remain a big challenge for quite a long time.

Conflicts of interest

There are no conflicts to declare.

Acknowledgements

This work was supported by the National Natural Science Foundation of China (No. 21575137).

References

1 R. Schlögl, *Angew. Chem., Int. Ed.*, 2003, **42**, 2004–2008.
2 S. Xu, D. C. Ashley, H.-Y. Kwon, G. R. Ware, C.-H. Chen, Y. Losovyj, X. Gao, E. Jakubikova and J. M. Smith, *Chem. Sci.*, 2018, **9**, 4950–4958.
3 A. Klerke, C. Christensen, J. Nørskov and T. Vegge, *J. Mater. Chem.*, 2008, **18**, 2304–2310.
4 I. Dybkjaer, *Ammonia, Catalysis and Manufacture*, ed. A. Nielsen, Springer, Heidelberg, 1995, pp. 199–308.
5 G. Marnellos and M. Stoukides, *Science*, 1998, **282**, 98–100.
6 C. Guo, J. Ran, A. Vasileff and S. Qiao, *Energy Environ. Sci.*, 2018, **11**, 45–56.
7 Q. Wang, Y. Lei, D. Wang and Y. Li, *Energy Environ. Sci.*, 2019, **12**, 1730–1750.
8 R. Zhao, H. Xie, L. Chang, X. Zhang, X. Zhu, X. Tong, T. Wang, Y. Luo, P. Wei, Z. Wang and X. Sun, *EnergyChem*, 2019, **1**, 100011.
9 K. A. Brown, D. F. Harris, M. B. Wilker, A. Rasmussen, N. Khadka, H. Hamby, D. Keable, G. Dukovic, J. W. Peters, L. C. Seefeldt and P. W. King, *Science*, 2016, **352**, 448–450.
10 M. A. Shipman and M. D. Symes, *Catal. Today*, 2017, **286**, 57–68.
11 N. Cao and G. Zheng, *Nano Res.*, 2018, **11**, 2992–3008.
12 H. K. Lee, C. S. L. Koh, Y. H. Lee, C. Liu, I. Y. Phang, X. Han, C.-K. Tsung and X. Y. Ling, *Sci. Adv.*, 2018, **4**, eaar3208.
13 M. A. Shipman and M. D. Symes, *Catal. Today*, 2017, **286**, 57–68.
14 Á. Logadóttir and J. K. Nørskov, *J. Catal.*, 2003, **220**, 273–279.
15 D. Bao, Q. Zhang, F. Meng, H. Zhong, M. Shi, Y. Zhang, J. Yan, Q. Jiang and X. Zhang, *Adv. Mater.*, 2017, **29**, 1604799.
16 J. Wang, L. Yu, L. Hu, G. Chen, H. Xin and X. Feng, *Nat. Commun.*, 2018, **9**, 1795.
17 H. Bielawa, O. Hinrichsen, A. Birkner and M. Muhler, *Angew. Chem., Int. Ed.*, 2001, **40**, 1061–1063.
18 D. Wang, L. M. Azofra, M. Harb, L. Cavallo, X. Zhang, B. H. R. Suryanto and D. R. MacFarlane, *ChemSusChem*, 2018, **11**, 3416–3422.
19 H. Huang, L. Xia, X. Shi, A. M. Asiri and X. Sun, *Chem. Commun.*, 2018, **54**, 11427–11430.
20 B. M. Hoffman, D. Lukoyanov, Z. Yang, D. R. Dean and L. C. Seefeldt, *Chem. Rev.*, 2014, **114**, 4041–4062.
21 R. R. Eady, *Chem. Rev.*, 1996, **96**, 3013–3030.
22 L. Zhang, X. Ji, X. Ren, Y. Ma, X. Shi, Z. Tian, A. M. Asiri, L. Chen, B. Tang and X. Sun, *Adv. Mater.*, 2018, **30**, 1800191.
23 L. Zhang, X. Ji, X. Ren, Y. Luo, X. Shi, A. M. Asiri, B. Zheng and X. Sun, *ACS Sustainable Chem. Eng.*, 2018, **6**, 9550–9554.
24 X. Ren, J. Zhao, Q. Wei, Y. Ma, H. Guo, Q. Liu, Y. Wang, G. Cui, A. M. Asiri, B. Li, B. Tang and X. Sun, *ACS Cent. Sci.*, 2019, **5**, 116–121.
25 H. Cheng, L. Ding, G. Chen, L. Zhang, J. Xue and H. Wang, *Adv. Mater.*, 2018, **30**, 1803694.
26 J. Han, X. Ji, X. Ren, G. Cui, L. Li, F. Xie, H. Wang, B. Li and X. Sun, *J. Mater. Chem. A*, 2018, **6**, 12974–12977.
27 S. Licht, B. Cui, B. Wang, F. Li, J. Lau and S. Liu, *Science*, 2014, **345**, 637–640.
28 S. Chen, S. Perathoner, C. Ampelli, C. Mebrahtu, D. Su and G. Centi, *Angew. Chem., Int. Ed.*, 2017, **56**, 2699–2703.
29 X. Xiang, Z. Wang, X. Shi, M. Fan and X. Sun, *ChemCatChem*, 2018, **10**, 4530–4535.
30 Q. Liu, X. Zhang, B. Zhang, Y. Luo, G. Cui, F. Xie and X. Sun, *Nanoscale*, 2018, **10**, 14386–14389.
31 L. Hu, A. Khaniya, J. Wang, G. Chen, W. E. Kaden and X. Feng, *ACS Catal.*, 2018, **8**, 9312–9319.
32 X. Zhao, X. Lan, D. Yu, H. Fu, Z. Liu and T. Mu, *Chem. Commun.*, 2018, **54**, 13010–13013.
33 X. Zhu, Z. Liu, Q. Liu, Y. Luo, X. Shi, A. M. Asiri, Y. Wu and X. Sun, *Chem. Commun.*, 2018, **54**, 11332–11335.
34 X. Zhu, T. Wu, L. Ji, Q. Liu, Y. Luo, G. Cui, Y. Xiang, Y. Zhang, B. Zheng and X. Sun, *Chem. Commun.*, 2020, DOI: 10.1039/c9cc08352a.
35 Y. Abghoui, A. L. Garden, J. G. Howalt, T. Vegge and E. Skúlason, *ACS Catal.*, 2016, **6**, 635–646.
36 R. Zhang, Y. Zhang, X. Ren, G. Cui, A. M. Asiri, B. Zheng and X. Sun, *ACS Sustainable Chem. Eng.*, 2018, **6**, 9545–9549.
37 X. Yang, J. Nash, J. Anibal, M. Dunwell, S. Kattel, E. Stavitski, K. Attenkofer, J. G. Chen, Y. Yan and B. Xu, *J. Am. Chem. Soc.*, 2018, **140**, 13387–13391.
38 X. Yang, S. Kattel, J. Nash, X. Chang, J. Lee, Y. Yan, J. Chen and B. Xu, *Angew. Chem., Int. Ed.*, 2019, **131**, 13906–13910.
39 R. Zhang, H. Guo, L. Yang, Y. Wang, Z. Niu, H. Huang, H. Chen, L. Xia, T. Li, X. Shi, X. Sun, B. Li and Q. Liu, *ChemElectroChem*, 2019, **6**, 1014–1018.
40 R. Zhang, J. Han, B. Zheng, X. Shi, A. M. Asiri and X. Sun, *Inorg. Chem. Front.*, 2019, **6**, 391–395.
41 R. Zhang, X. Ren, X. Shi, F. Xie, B. Zheng, X. Guo and X. Sun, *ACS Appl. Mater. Interfaces*, 2018, **10**, 28251–28255.
42 G. Yu, H. Guo, W. Kong, T. Wang, Y. Luo, X. Shi, A. M. Asiri, T. Li and X. Sun, *J. Mater. Chem. A*, 2019, **7**, 19657–19661.
43 Y. Luo, G. Chen, L. Ding, X. Chen, L. Ding and H. Wang, *Joule*, 2019, **3**, 279–289.
44 L. Huang, J. Wu, P. Han, A. M. Al-Enizi, T. M. Almutairi, L. Zhang and G. Zheng, *Small Methods*, 2019, **3**, 1800386.
45 J. Han, Z. Liu, Y. Ma, G. Cui, F. Xie, F. Wang, Y. Wu, S. Gao, Y. Xu and X. Sun, *Nano Energy*, 2018, **52**, 264–270.
46 Y. Zhang, W. Qiu, Y. Ma, Y. Luo, Z. Tian, G. Cui, F. Xie, L. Chen, T. Li and X. Sun, *ACS Catal.*, 2018, **8**, 8540–8544.

47 Z. Wang, F. Gong, L. Zhang, R. Wang, L. Ji, Q. Liu, Y. Luo, H. Guo, Y. Li, P. Gao, X. Shi, B. Li, B. Tang and X. Sun, *Adv. Sci.*, 2019, **6**, 1801182.

48 K. Chu, Y. Liu, Y. Li, H. Zhang and Y. Tian, *J. Mater. Chem. A*, 2019, **7**, 4389–4394.

49 C. Li, S. Mou, X. Zhu, F. Wang, Y. Wang, Y. Qiao, X. Shi, Y. Luo, B. Zheng, Q. Li and X. Sun, *Chem. Commun.*, 2019, **55**, 14474–14477.

50 L. Li, C. Tang, B. Xia, H. Jin, Y. Zheng and S. Qiao, *ACS Catal.*, 2019, **9**, 2902–2908.

51 R. Zhang, L. Ji, W. Kong, H. Wang, R. Zhao, H. Chen, T. Li, B. Li, Y. Luo and X. Sun, *Chem. Commun.*, 2019, **55**, 5263–5266.

52 L. Zhang, X. Ren, Y. Luo, X. Shi, A. M. Asiri, T. Li and X. Sun, *Chem. Commun.*, 2018, **54**, 12966–12969.

53 P. Li, Z. Liu, T. Wu, Y. Zhang, L. Wang, L. Wang, L. Ji, Y. Zhang, Y. Luo, T. Wang, S. Liu, Y. Wu, M. Liu and X. Sun, *J. Mater. Chem. A*, 2019, **7**, 17761–17765.

54 J. Deng, M. Li and Y. Wang, *Green Chem.*, 2016, **18**, 4824–4854.

55 X. Zhang, T. Wu, H. Wang, R. Zhao, H. Chen, T. Wang, P. Wei, Y. Luo, Y. Zhang and X. Sun, *ACS Catal.*, 2019, **9**, 4609–4615.

56 Q. Fan, C. Choi, C. Yan, Y. Liu, J. Qiu, S. Hong, Y. Jung and Z. Sun, *Chem. Commun.*, 2019, **55**, 4246–4249.

57 L. Zhang, L. Ding, G. Chen, X. Yang and H. Wang, *Angew. Chem., Int. Ed.*, 2019, **58**, 2612–2616.

58 W. Qiu, X. Xie, J. Qiu, W. Fang, R. Liang, X. Ren, X. Ji, G. Cui, A. M. Asiri, G. Cui, B. Tang and X. Sun, *Nat. Commun.*, 2018, **9**, 3485.

59 X. Zhu, T. Wu, L. Ji, C. Li, T. Wang, S. Wen, S. Gao, X. Shi, Y. Luo, Q. Peng and X. Sun, *J. Mater. Chem. A*, 2019, **7**, 16117–16121.

60 J. Zhao, X. Ren, X. Li, D. Fan, X. Sun, H. Ma, Q. Wei and D. Wu, *Nanoscale*, 2019, **11**, 4231–4235.

61 Y. Zhang, H. Du, Y. Ma, L. Ji, H. Guo, Z. Tian, H. Chen, H. Huang, G. Cui, A. M. Asiri, F. Qu, L. Chen and X. Sun, *Nano Res.*, 2019, **12**, 919–924.

62 C. Lv, Y. Qian, C. Yan, Y. Ding, Y. Liu, G. Chen and G. Yu, *Angew. Chem., Int. Ed.*, 2018, **57**, 10246–10250.

63 Y. Yang, M. Luo, W. Zhang, Y. Sun, X. Chen and S. Guo, *Chem*, 2018, **4**, 2054–2083.

64 S. Dou, X. Wang and S. Wang, *Small Methods*, 2019, **3**, 1800211.

65 C. Li, T. Wang, Z. Zhao, W. Yang, J. Li, A. Li, Z. Yang, G. A. Ozin and J. Gong, *Angew. Chem., Int. Ed.*, 2018, **57**, 5278–5282.

66 L. Yang, T. Wu, R. Zhang, H. Zhou, L. Xia, X. Shi, H. Zheng, Y. Zhang and X. Sun, *Nanoscale*, 2019, **11**, 1555–1562.

67 L. Zhang, X. Xie, H. Wang, L. Ji, Y. Zhang, H. Chen, T. Li, Y. Luo, G. Cui and X. Sun, *Chem. Commun.*, 2019, **55**, 4627–4630.

68 W. Kong, R. Zhang, X. Zhang, L. Ji, G. Yu, T. Wang, Y. Luo, X. Shi, Y. Xu and X. Sun, *Nanoscale*, 2019, **11**, 19274–19277.

69 X. Cui, C. Tang, X. Liu, C. Wang, W. Ma and Q. Zhang, *Chem.–Eur. J.*, 2018, **24**, 18494–18501.

70 B. Xu, L. Xia, F. Zhou, R. Zhao, H. Chen, T. Wang, Q. Zhou, Q. Liu, G. Cui, X. Xiong, F. Gong and X. Sun, *ACS Sustainable Chem. Eng.*, 2019, **7**, 2889–2893.

71 H. Jin, L. Li, X. Liu, C. Tang, W. Xu, S. Chen, L. Song, Y. Zheng and S. Qiao, *Adv. Mater.*, 2019, **31**, 1902709.

72 J. D. Benck, T. R. Hellstern, J. Kibsgaard, P. Chakthranont and T. F. Jaramillo, *ACS Catal.*, 2014, **4**, 3957–3971.

73 X. Li, T. Li, Y. Ma, Q. Wei, W. Qiu, H. Guo, X. Shi, P. Zhang, A. M. Asiri, L. Chen, B. Tang and X. Sun, *Adv. Energy Mater.*, 2018, **8**, 1801357.

74 Y. Wang, M. Shi, D. Bao, F. Meng, Q. Zhang, Y. Zhou, K. Liu, Y. Zhang, J. Wang, Z. Chen, D. Liu, Z. Jiang, M. Luo, L. Gu, Q. Zhang, X. Cao, Y. Yao, M. Shao, Y. Zhang, X. Zhang, J. Chen, J. Yan and Q. Jiang, *Angew. Chem., Int. Ed.*, 2019, **58**, 9464–9469.

75 Y. Liu, Y. Su, X. Quan, X. Fan, S. Chen, H. Yu, H. Zhao, Y. Zhang and J. Zhao, *ACS Catal.*, 2018, **8**, 1186–1191.

76 H. Wang, L. Wang, Q. Wang, S. Ye, W. Sun, Y. Shao, Z. Jiang, Q. Qiao, Y. Zhu, P. Song, D. Li, L. He, X. Zhang, J. Yuan, T. Wu and G. A. Ozin, *Angew. Chem., Int. Ed.*, 2018, **57**, 12360–12364.

77 X. Yu, P. Han, Z. Wei, L. Huang, Z. Gu, S. Peng, J. Ma and G. Zheng, *Joule*, 2018, **2**, 1610–1622.

78 T. Wang, L. Xia, J. Yang, H. Wang, W. Fang, H. Chen, D. Tang, A. M. Asiri, Y. Luo, G. Cui and X. Sun, *Chem. Commun.*, 2019, **55**, 7502–7505.

79 L. Xia, J. Yang, H. Wang, R. Zhao, H. Chen, W. Fang, A. M. Asiri, F. Xie, G. Cui and X. Sun, *Chem. Commun.*, 2019, **55**, 3371–3374.

80 J. Zhao, J. Yang, L. Ji, H. Wang, H. Chen, Z. Niu, Q. Liu, Ti. Li, G. Cui and X. Sun, *Chem. Commun.*, 2019, **55**, 4266–4269.

81 X. Zhu, Z. Liu, H. Wang, R. Zhao, H. Chen, T. Wang, F. Wang, Y. Luo, Y. Wu and X. Sun, *Chem. Commun.*, 2019, **55**, 3987–3990.

82 Y. Liu, Y. Li, H. Zhang and K. Chu, *Inorg. Chem.*, 2019, **58**, 10424–10431.

83 S. Zhang, C. Zhao, Y. Liu, W. Li, J. Wang, G. Wang, Y. Zhang, H. Zhang and H. Zhao, *Chem. Commun.*, 2019, **55**, 2952–2955.

84 K. Jia, Y. Wang, Q. Pan, B. Zhong, Y. Luo, G. Cui, X. Guo and X. Sun, *Nanoscale Adv.*, 2019, **1**, 961–964.

85 Q. Qin, Y. Zhao, M. Schmallegger, T. Heil, J. Schmidt, R. Walczak, G. Demner, H. Jiao and M. Oschatz, *Angew. Chem., Int. Ed.*, 2019, **58**, 13101–13106.

86 Y. Wang, K. Jia, Q. Pan, Y. Xu, Q. Liu, G. Cui, X. Guo and X. Sun, *ACS Sustainable Chem. Eng.*, 2019, **7**, 117–122.

87 T. Wu, W. Kong, Y. Zhang, Z. Xing, J. Zhao, T. Wang, X. Shi, Y. Luo and X. Sun, *Small Methods*, 2019, **3**, 1900356.

88 N. Cao, Z. Chen, K. Zang, J. Xu, J. Zhong, J. Luo, X. Xu and G. Zheng, *Nat. Commun.*, 2019, **10**, 2877.

89 T. Wu, X. Zhu, Z. Xing, S. Mou, C. Li, Y. Qiao, Q. Liu, Y. Luo, X. Shi, Y. Zhang and X. Sun, *Angew. Chem., Int. Ed.*, 2019, **131**, 18620–18624.

90 J. Zhao, B. Wang, Q. Zhou, H. Wang, X. Li, H. Chen, Q. Wei, D. Wu, Y. Luo, J. You, F. Gong and X. Sun, *Chem. Commun.*, 2019, **55**, 4997–5000.

91 Y. Song, T. Wang, J. Sun, Z. Wang, Y. Luo, L. Zhang, H. Ye and X. Sun, *ACS Sustainable Chem. Eng.*, 2019, **7**, 14368–14372.

92 G. Deng, T. Wang, A. A. Alshehri, K. A. Alzahrani, Y. Wang, H. Ye, Y. Luo and X. Sun, *J. Mater. Chem. A*, 2019, **7**, 21674–21677.

93 S. Li, D. Bao, M. Shi, B. Wulan, J. Yan and Q. Jiang, *Adv. Mater.*, 2017, **29**, 1700001.

94 C. Lv, C. Yan, G. Chen, Y. Ding, J. Sun, Y. Zhou and G. Yu, *Angew. Chem., Int. Ed.*, 2018, **57**, 6073.

95 Z. Xue, S. Zhang, Y. Lin, H. Su, G. Zhai, J. Han, Q. Yu, X. Li, M. Antonietti and J. Chen, *J. Am. Chem. Soc.*, 2019, **141**, 14976–17980.

96 M. Shi, D. Bao, B. Wulan, Y. Li, Y. Zhang, J. Yan and Q. Jiang, *Adv. Mater.*, 2017, **29**, 1606550.

97 Z. Wang, Y. Li, H. Yu, Y. Xu, H. Xue, X. Li, H. Wang and L. Wang, *ChemSusChem*, 2018, **11**, 3480–3485.

98 M. Nazemi, S. R. Panikkanvalappil and M. A. El-Sayed, *Nano Energy*, 2018, **49**, 316–323.

99 X. Zhang, Q. Liu, X. Shi, A. M. Asiri, Y. Luo, X. Sun and T. Li, *J. Mater. Chem. A*, 2018, **6**, 17303–17306.

100 H. Huang, F. Gong, Y. Wang, H. Wang, X. Wu, W. Lu, R. Zhao, H. Chen, X. Shi, A. M. Asiri, T. Li, Q. Liu and X. Sun, *Nano Res.*, 2019, **12**, 1093–1098.

101 L. Xia, B. Li, Y. Zhang, R. Zhang, L. Ji, H. Chen, G. Cui, H. Zheng, X. Sun, F. Xie and Q. Liu, *Inorg. Chem.*, 2019, **58**, 2257–2260.

102 K. Chu, Y. Liu, Y. Li, J. Wang and H. Zhang, *ACS Appl. Mater. Interfaces*, 2019, **11**, 31806–31815.

103 J. Li, X. Zhu, T. Wang, Y. Luo and X. Sun, *Inorg. Chem. Front.*, 2019, **6**, 2682–2685.

104 X. Zhu, J. Zhao, L. Ji, T. Wu, T. Wang, S. Gao, A. A. Alshehri, K. A. Alzahrani, Y. Luo, Y. Xiang, B. Zheng and X. Sun, *Nano Res.*, 2019, DOI: 10.1007/s12274-019-2600-8.

105 M. Shi, D. Bao, S. Li, B. Wulan, J. Yan and Q. Jiang, *Adv. Energy Mater.*, 2018, **8**, 1800124.

106 H. Xie, Q. Geng, X. Zhu, Y. Luo, L. Chang, X. Niu, X. Shi, A. M. Asiri, S. Gao, Z. Wang and X. Sun, *J. Mater. Chem. A*, 2019, **7**, 24760–24764.

107 R. Zhao, C. Liu, X. Zhang, X. Zhu, P. Wei, L. Ji, Y. Guo, S. Gao, Y. Luo, Z. Wang and X. Sun, *J. Mater. Chem. A*, 2019, **1**, 100011.

108 H. Chen, X. Zhu, H. Huang, H. Wang, T. Wang, R. Zhao, H. Zheng, A. M. Asiri, Y. Luo and X. Sun, *Chem. Commun.*, 2019, **55**, 3152–3155.

109 P. Li, J. Wang, H. Chen, X. Sun, J. You, S. Liu, Y. Zhang, M. Liu, X. Niu and Y. Luo, *J. Mater. Chem. A*, 2019, **7**, 12446–12450.

110 B. Anasori, M. R. Lukatskaya and Y. Gogotsi, *Nat. Rev. Mater.*, 2017, **2**, 16098.

111 J. Zhao, L. Zhang, X. Xie, X. Li, Y. Ma, Q. Liu, W. Fang, X. Shi, G. Cui and X. Sun, *J. Mater. Chem. A*, 2018, **6**, 24031–24035.

112 W. Kong, F. Gong, Q. Zhou, G. Yu, L. Ji, X. Sun, A. M. Asiri, T. Wang, Y. Luo and Y. Xu, *J. Mater. Chem. A*, 2019, **7**, 18823–18827.

113 Y. Fang, Z. Liu, J. Han, Z. Jin, Y. Han, F. Wang, Y. Niu, Y. Wu and Y. Xu, *Adv. Energy Mater.*, 2019, **9**, 1803406.

114 Y. Liu, D. Li, J. Yu and B. Ding, *Angew. Chem., Int. Ed.*, 2019, **58**, 1–7.

115 Y. Chen, S. Ji, C. Chen, Q. Peng, D. Wang and Y. Li, *Joule*, 2018, **2**, 1242–1264.

116 X. Wang, W. Wang, M. Qiao, G. Wu, W. Chen, T. Yuan, Q. Xue, M. Chen, Y. Zhang, X. Wang, J. Wang, J. Ge, X. Hong, Y. Li, Y. Wu and Y. Li, *Sci. Bull.*, 2018, **63**, 1246–1253.

117 Q. Qin, T. Heil, M. Antonietti and M. Oschatz, *Small Methods*, 2018, **2**, 1800202.

118 Z. Geng, Y. Liu, X. Kong, P. Li, K. Li, Z. Liu, J. Du, M. Shu, R. Si and J. Zeng, *Adv. Mater.*, 2018, **30**, 1803498.

119 L. Han, X. Liu, J. Chen, R. Lin, H. Liu, F. Lü, S. Bak, Z. Liang, S. Zhao, E. Stavitski, J. Luo, R. R. Adzic and H. L. Xin, *Angew. Chem., Int. Ed.*, 2019, **58**, 2321–2325.

120 M. Wang, S. Liu, T. Qian, J. Liu, J. Zhou, H. Ji, J. Xiong, J. Zhong and C. Yan, *Nat. Commun.*, 2019, **10**, 341.

121 Y. Wang, X. Cui, Y. Zhang, L. Zhang, X. Gong and G. Zheng, *Adv. Mater.*, 2016, **28**, 7626–7632.

122 G. Chen, X. Cao, S. Wu, X. Zeng, L. Ding, M. Zhu and H. Wang, *J. Am. Chem. Soc.*, 2017, **139**, 9771–9774.

123 Y. Liu, M. Han, Q. Xiong, S. Zhang, C. Zhao, W. Gong, G. Wang, H. Zhang and H. Zhao, *Adv. Energy Mater.*, 2019, **9**, 1803935.

124 Y. Hao, Y. Guo, L. Chen, M. Shu, X. Wang, T. Bu, W. Gao, N. Zhang, X. Su, X. Feng, J. Zhou, B. Wang, C. Hu, A. Yin, R. Si, Y. Zhang and C. Yan, *Nat. Catal.*, 2019, **2**, 448–456.

125 Y. Mukouyama, R. Nakazato, T. Shiono, S. J. Nakanishi and H. Okamoto, *J. Electroanal. Chem.*, 2014, **713**, 39–46.

126 Y. Yang, S. Wang, H. Wen, T. Ye, J. Chen, C. Li and M. Du, *Angew. Chem., Int. Ed.*, 2019, **131**, 15506–15510.

127 D. Strmcnik, P. P. Lopes, B. Genorio, V. R. Stamenkovic and N. M. Markovic, *Nano Energy*, 2016, **29**, 29–36.

128 L. F. Greenlee, J. N. Renner and S. L. Foster, *ACS Catal.*, 2018, **8**, 7820–7827.

129 S. Z. Andersen, V. Čolić, S. Yang, J. A. Schwalbe, A. C. Nielander, J. M. McEnaney, K. Enemark-Rasmussen, J. G. Baker, A. R. Singh, B. A. Rohr, M. J. Statt, S. J. Blair, S. Mezzavilla, J. Kibsgaard, P. C. K. Vesborg, M. Cargnello, S. F. Bent, T. F. Jaramillo, I. E. L. Stephens, J. K. Nørskovand and I. Chorkendorff, *Nature*, 2019, **570**, 504–508.

130 C. Tang and S. Qiao, *Joule*, 2019, **3**, 1573–1575.

131 H. Du, T. R. Gengenbach, R. Hodgetts, D. R. MacFarlane and A. N. Simonov, *ACS Sustainable Chem. Eng.*, 2019, **7**, 6839–6850.